BULLETIN OF THE POLISH ACADEMY OF SCIENCES
TECHNICAL SCIENCES, Vol. 63, No. 4, 2015
DOI: 10.1515/bpasts-2015-0099

Numerical study of selected military vehicle chassis subjected to blast loading in terms of tire strength improving

P. BARANOWSKI* and J. MALACHOWSKI

Department of Mechanics and Applied Computer Science, Military University of Technology,
2 Gen. Sylwestra Kaliskiego St., 00-908 Warsaw, Poland

Abstract. In the paper a chosen model of the light armoured vehicle was tested in terms of blast loading. More precisely, the blast propagation and interaction with the tire behaviour and suspension system elements of the light-armoured vehicle (LAV) was simulated. The chosen military vehicle meets the requirements of levels 2A and 2B of STANAG 4569 standard. Based on the obtained results, two modifications were proposed for the strength and resistance improvement of the wheel. The first consisted of inserting the rubber runflat ring inside the tire, whereas in the second the honeycomb-like composite wheel was implemented. Non-linear dynamic simulations were carried out using the explicit LS-Dyna code, with multi- material Arbitrary Lagrangian-Eulerian formulation for simulation the blast process.

Key words: blast loading, LAV, tire, FE analysis.

1. Introduction

Recent events have shown that in many world military operations Improvised Explosive Devices (IED) are commonly used on battlefields. Its destructive effect manifests in a tire tearing followed by a large deformation of other suspension system elements [1–3]. Moreover, formed blast wave reflects from a motor-car body bottom surface instead of dissipating dealing with more overall damage to vehicle chassis. The procedures of blast wave interaction with military vehicles are defined in STANAG 4569 standardization of protection levels for occupants of logistic and light armoured vehicles [4].

Problems of blast wave interaction with vehicle structures have been commonly simulated using numerical methods [5–10]. Basically the explicit Finite Element (FE) code is used with three major methods of blast loading modelling implementation: ConWep function [5, 6], Smoothed Particle Hydrodynamics (SPH) method [7, 8] and the most sophisticated multi material Arbitrary Lagrangian-Eulerian (MM-ALE) formulation [9, 10] procedure, which was also adopted in the presented paper.

The destructive process under- blast- loaded vehicle usually initiates within a wheel area. Therefore, for effective and correct analyses a numerical model of it should be developed with particular attention and care. The authors of the papers [11–15] present conceptions of the discrete tire modelling and the validation process. An accurate assessment of the tire rubber mechanical properties in various operational conditions is essential in the tire numerical modelling, which turns out to have a significant impact on the results [16]. Tire is a very complex structure consisting of several interconnected elementary parts with different material parameters, i.e. a sidewall, a tread, a bead core, etc. [11, 13, 14, 16, 17] and strengthening layers made of parallel fibres which can be made of polyester, nylon or steel. Immersed in the rubber with different orientations, they form a special ring-like laminate. One can find that most authors use a simplified technique [18, 19] or complex method [20, 21] for tire discretization, both with overall good correlation with the experiments.

The genesis of the paper is related to the problem of simulation of blast wave interaction with a vehicle. However, the authors found a lack of material data of tire rubber with a wide range of the stress-strain curves within a number of strain rates, especially in terms of dynamic loading analyses. In the presented tire modelling concept the Simplified Rubber (SR) model [22] was used with all the stress-strain experimental data implemented as a table containing all the curves for the corresponding strain rate. Such a material model with proper and validated stress-strain curves is universal for various problems considering rubber modelling not only in the dynamic conditions, but also in problems with quasi-static nature.

In the paper, a selected suspension system was loaded with a blast wave (according to STANAG 4569 level 2A and 2B) and dynamic behaviour of the tire and its failure was examined with the energy dissipation taking into account. Therefore, the runflat ring and the honeycomb composite structure were introduced and their effect on lowering the pressure wave energy was examined.

2. Object of investigations

The suspension system was developed based on the real off-road military vehicle elements [5, 23, 24] (Fig. 1). It mainly consists of: a chassis frame part, a spring, an axle, an axle bush, a hub, a drum brake, a drum brake pads, a steel rim and a wheel. Geometry of the tire and other suspension elements was achieved thanks to the reverse engineering technology. The tire was divided into six different parts, with material

*e-mail: pawel.baranowski@wat.edu.pl

properties of the carcass and the inner fabric taken from the literature [25] (Table 1). For all steel components the simplified Johnson-Cook (JC) constitutive model was used, with literature parameters [26] (Table 2). Rubber components were described using the SR model [22] with the implemented family of stress-strain curves for different strain rates obtained from quasi-static and dynamic tests performed using universal strength machines and split Hopkinson pressure bar (SHPB) with aluminium and polyacrylate (PMMA) bars [27] (Fig. 2). The FE model of the tire was validated with the actual one, as presented in the authors paper [15].

Fig. 1. Suspension system and tire used in investigations

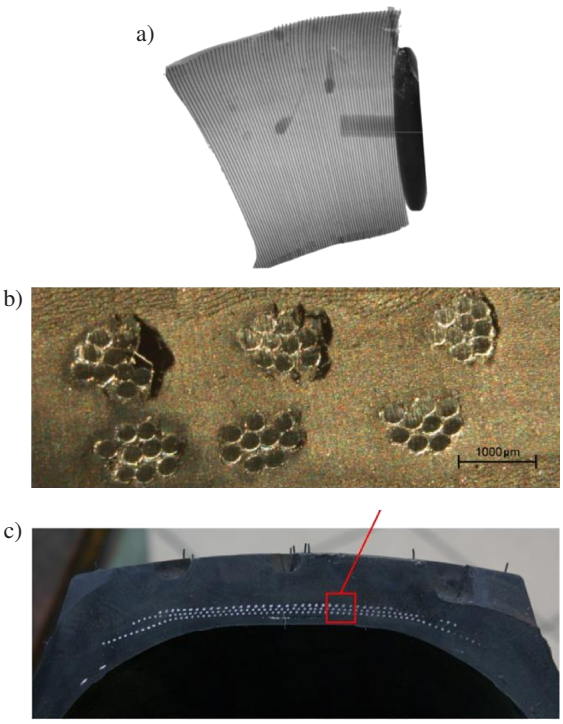

Fig. 2. a) CT scan photography of cords pattern in tire sidewall, b) tread cords pattern in microscale, c) cords pattern in tire tread Refs. (5,15,23,24)

Table 1
Orthotropic components materials data (Ref. 25)

	E [MPa]			ρ [kg/m^3]	Poisson's ratio ν		
	E_1	E_2	E_3		ν_{12}	ν_{13}	ν_{23}
Carcass	107	127	107	1351	0.451	0.0038	0.0038
Inner fabric	3181	83	83	2497	0.00011	0.00011	0.454

Table 2
Steel parameters for simplified JC model used in analyses (Ref. 26)

ρ [kg/m^3]	A_{JC} [MPa]	B_{JC} [MPa]	C_{JC}	r	Ps_{fail}
7850	365	510	0.0936	0.90	0.30

An exact tire cords pattern was achieved thanks to computed tomography (CT) scanning. As it can be seen in Fig. 2, steel cords are arranged radially inside a tire sidewall, whereas within tread area they are placed circumferentially. A single cord consists of 9 smaller wires, with their average total measured diameter of ∼1.2 mm (Fig. 2b). Moreover, the rubber-steel cords volumetric ratio was verified, which was taken into account in numerical tire modelling. In the next stages, it was adopted into a developed discrete model of the wheel. Moreover, verification of the cords layout inside the tire structure allowed the authors to prepare specimens for rubber experimental testing without the cords.

In the performed studies, the suspension system with a simplified chassis of vehicle was taken into consideration. It was represented by a non-deformable surface modelled with 11266 Belytschko-Tsay (BT) shell elements [28] and 11455 nodes with 25% of vehicle mass associated. For the tire and other suspension system parts modelling brick elements with one integration point were adopted (constant stress solid elements) which are recommended for large deformation analyses [28]. Such a solid formulation is default in the explicit software and is efficient and accurate, however hourglass control needs to be used in almost every case. Steel cords were modelled using truss (cable) elements which have three degrees of freedom at each node and carry only axial force [28]. The diameter of 1.20 mm measured from the microscopic photo was used. The FE model of suspension system reached 59633 brick and truss elements and 87108 nodes. Table 3 presents the suspension system parts statistic data, whereas in Table 4 the statistic data of the tire is presented. The geometrical representation of the analysed discrete model is shown in Fig. 3 [5, 23, 24].

Table 3
Statistic data of discrete suspension system model (Refs. 23, 24)

	No. of hexagonal elements	No. of nodes
Tread	3840	6360
Inner fabric	3600	7680
Carcass	1680	3600
Sidewall	4800	8160
Bead core	2400	3840
	No of truss elements	No. of nodes
Circumferential cords	4560	4561
Radial cords	8639	8881

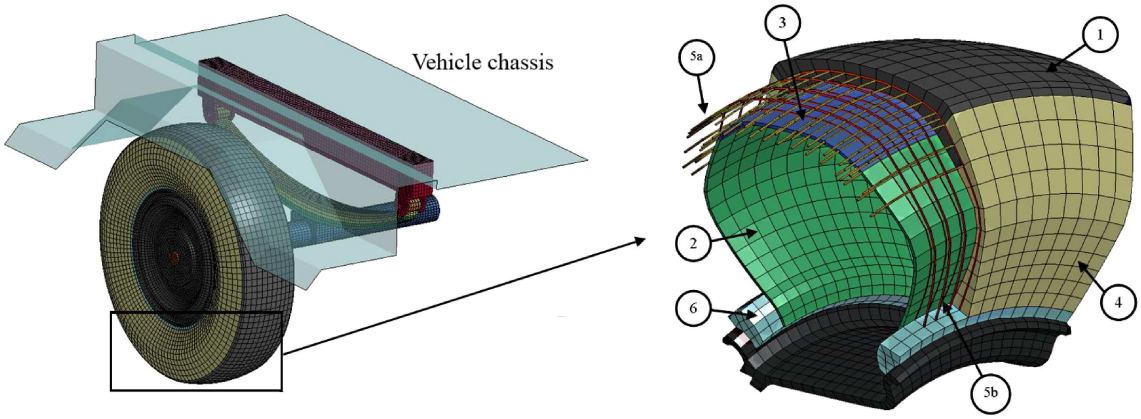

Fig. 3. FE suspension system model and tire components Refs. (5,15,23,24) (1. Tread, 2. Inner fabric, 3. Carcass, 4. Sidewall, 5a. Circumferential cords, 5b. Radial cords, 6. Bead core with cords)

Table 4
Statistic data of discrete tire model (Refs. 23, 24)

	No. of hexagonal elements	No. of nodes
Tire	16320	25520
Rim	7192	12164
Drum brake	4680	7440
Axle	4278	5236
Hub	2268	3132
Axle bush	4585	6207
Spring	4368	7077
Chassis frame part	7302	9052
	No. of shell elements	No. of nodes
Chassis	11266	11455

3. Numerical studies

Numerical analyses were performed using the explicit code using MM-ALE. All tire and suspension system parts were embedded in the Eulerian air domain. In order to minimize the computation time and increase the computational efficiency, only one wheel and 1/4 of the vehicle body was modelled with symmetry conditions applied correspondingly at the end of the axle and at the end of surface representing the chassis. Mesh density was selected through a number of the analyses in order to guarantee high accuracy of computations and reasonable simulation time. Such sensitivity studies have to be performed before the final simulations, due to possible significant differences in the results depending on the mesh properties, which was also discussed in the papers of other authors [29, 30]. Pressure inside the tire was represented by the airbag model (Green's function closed volume integration [28]). For numerical tire destruction the erosion criteria were implemented based on the effective strain failure variable taken from the quasi-static tension test (see Fig. 4). The air was considered as a simple ideal gas with the vacuum constitutive model parameters.

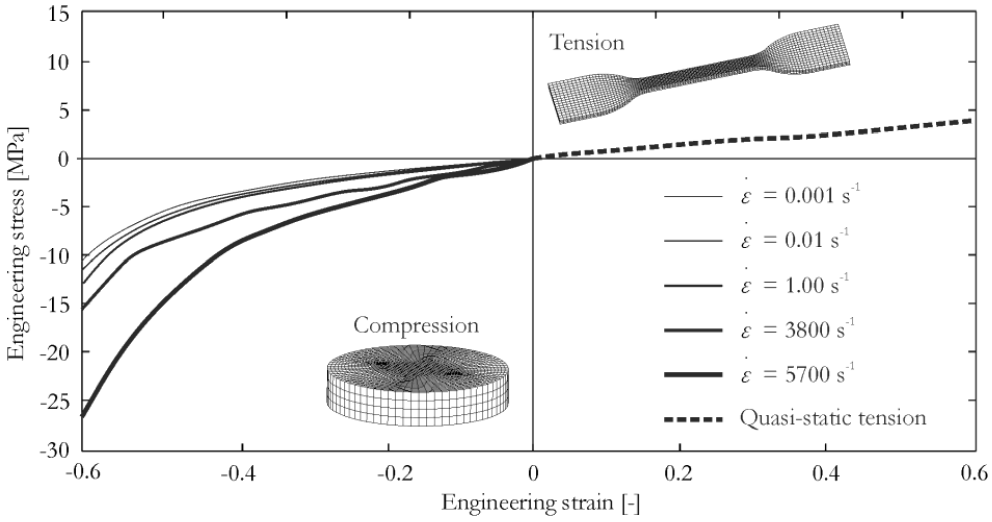

Fig. 4. Engineering stress vs. strain curves used in rubber components described with SR constitutive model, Ref. 27

In the simulations, it was necessary to implement the detonation process of the high explosive material into the model using the so called "explosive burn" material model. In this approach, the energy from the explosion phenomenon is assumed to be suddenly released inside the front of detonation wave. The detonation process requires to model a movement of the products of detonation (PD) after they reach subsequent specific locations by the detonation wave (DW) front. Material parameters for the TNT charge were calculated analytically supplemented by data from the literature [26, 27] (Table 5). The Jones Wilkins Lee (JWL) equation of state with the following form was used [28]:

$$p = A\left(1 - \frac{\omega}{R_1\overline{\rho}}\right)\exp\left(-R_1\overline{\rho}\right) + B\left(1 - \frac{\omega}{R_2\overline{\rho}}\right)\exp\left(-R_2\overline{\rho}\right) + \frac{\omega\overline{e}}{\overline{\rho}}, \tag{1}$$

where $\overline{\rho} = \rho_{HE}/\rho$, $\overline{e} = \rho_{HE}e$, ρ_{HE} – density of the high explosive, p – pressure, e – specific internal energy, ρ – density of detonation product. A, B, R_1, R_2, ω – empirical constants determined for specific type of an explosive material.

Table 5
TNT parameters for HE material and JWL equation of state (Refs. 26, 27)

ρ_{HE} [kg/m^3]	D [m/s]	A_{HE} [MPa]	B_{HE} [MPa]	R_1 [–]	R_2 [–]	ω [–]	E_0 [J/mm^3]
1580	6930	3.712e+4	3.712e+3	4.15	0.90	0.35	

The interaction between pressure wave, vacuum and Lagrangian parts (also between each of them) was simulated using the coupling procedure based on the penalty method [28] and the second order advection procedure was implemented [28] in Eulerian domain.

The simulation of the suspension system subjected to blast wave loading was carried out with the initial-boundary conditions according to STANAG 4569 standardization of the protection level 2A [4], which are as follows:

- The HE is placed under the wheel offset towards the vehicle and its placement was evaluated based on the formula:

$$S/2 \leq d \leq 0.4(S + D), \tag{2}$$

  where S – wheel print width, d – distance between mine centre and wheel centre, D – diameter of charge;
- The HE is a short cylinder with a height to diameter ratio of 0.33: in the discussed analysis the 6 kg mine (TNT) was used with diameter D = 250 mm and height H = 80 mm;
- The *DoB* (Depth of Burial) for the mine is 100 mm;
- The HE is placed inside the soil.

The FE model for the suspension system without any modification with the initial-boundary conditions is presented in Fig. 5. The soil and the air were modelled using Eulerian elements with the HE representation by the initial volume fraction geometry option. For the soil, the material parameters were taken from literature [31] and the appropriate constitutive model was adopted (Soil and Foam Failure model [28]) with the data listed in Table 6.

Table 6
Material data for soil material (Ref. 31)

ρ [kg/m^3]	G [MPa]	Bulk [MPa]	Ao [–]	A1 [–]	A2 [–]	PC [–]	VCR [–]		
1255	1.724	5.516	0.00	0.00	0.87	0.00	0.00		
eps1 [–]	eps2 [–]	eps3 [–]	eps4 [–]	eps5 [–]	eps6 [–]	eps7 [–]	eps8 [–]	eps9 [–]	eps10 [–]
0.00	0.03	0.06	0.10	0.14	0.17	0.21	0.25	0.29	0.33
p1 [MPa]	p2 [MPa]	p3 [MPa]	p4 [MPa]	p5 [MPa]	p6 [MPa]	p7 [MPa]	p8 [MPa]	p9 [MPa]	p10 [MPa]
0.00	0.02	0.03	0.05	0.06	0.08	0.12	0.20	0.33	0.50

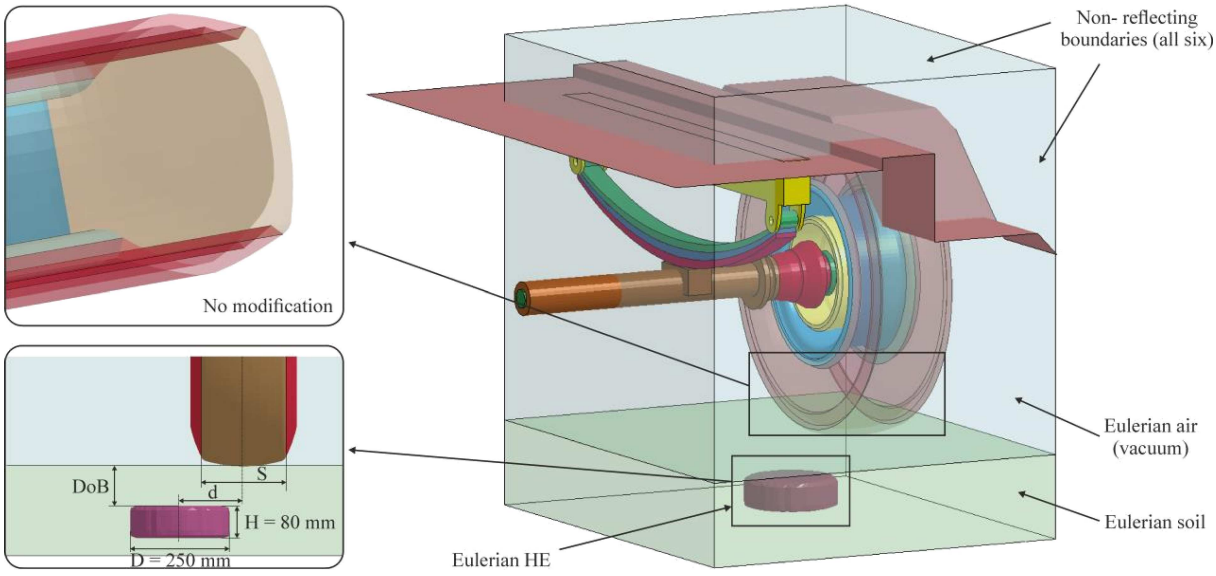

Fig. 5. Initial-boundary conditions for simulation with "severe" suspension system (case 1)

3.1. Wheel modifications. The first modification (case 2) consisted in inserting the rubber runflat ring which is very often used nowadays in public transport and in military vehicles [32, 33]. The insert geometry was taken from the actual one which was used in the light amour vehicle and was achieved using the reverse engineering technology (3D laser scanning). Based on the obtained polygons the CAD model and consequently the discrete model of the runflat ring was developed. In the actual conditions, the ring was made of rubber which has the same parameters as the tread of the tire. Therefore, during simulations the same material constitutive model with identical data for the other rubber-like parts was used. For the modelling, the eight-node brick elements with the one point reduced integration scheme were adopted [28]. The part consisted of 8640 elements and 11280 nodes, with mesh density matching the mesh of the rim for the proper connection (equivalence) between these parts. Moreover, an additional contact procedure with eroding option was added which allowed for simulating the interaction between runflat ring and other suspension system parts. The FE model of described configuration is presented in Fig. 6.

a)

b)

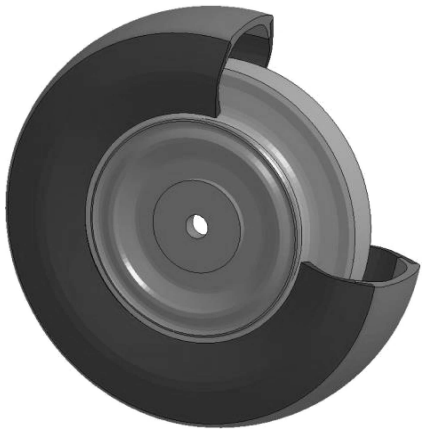

Fig. 6. Runflat insert used in investigations, a) actual wheel, b) discrete model

In the second modification (case 3), the honeycomb-like composite wheel was adopted. Such a solution is now widely used in military vehicles and is also known as a non-pneumatic tire [34, 35]. Such an airless wheel using a honeycomb-like internal structure has a lot of advantages in terms of safety and blast pressure wave strength with its ability to dissipate the energy. It provides both structural rigidity as well as flexibility. Based on the structure, which has been already manufactured, a discrete model of such a type was developed and applied into the FE model of the suspension system (Fig. 7). The composite structure was discretized using 4-node BT shell elements (18240 elements and 18912 nodes). Interaction between the composite insert and other suspension system parts was also simulated with the contact procedure and with added eroding option. The orthotropic material model with model failure mechanisms was applied (Enhanced Composite Damage model [28]). The material properties of fiber reinforced composite (FRC) used in simulations are listed in Table 7 [36].

a)

b)

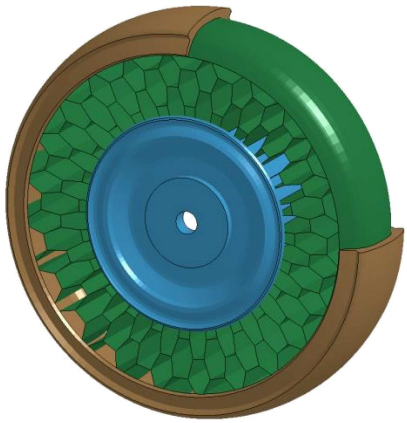

Fig. 7. Airless honeycomb tire used in investigations, a) actual wheel [34, 35], b) discrete model

Table 7
Material data for FRC (Ref. 36)

$E_1^t = E_2^t$ [MPa]	$E_1^c = E_2^c$ [MPa]	ν_{12} [–]	G_{12} [MPa]	G_{13} [MPa]	$R_1^t = R_2^t$ [MPa]
31900	31900	0.09	2370	780	474
$R_1^c = R_2^c$ [MPa]	S_{12} [MPa]	S_{13} [MPa]	$e_1^t = e_2^t$ [–]	$e_1^c = e_2^c$ [–]	
332	41.90	33.70	0.013	0.0115	

4. Results and discussion

During the simulations, concerning the suspension system loading using the blast pressure wave from the HE detonation, the following issues were investigated [27]:

- overall response and damage of structure (especially tire),
- influence of used modifications in terms of blast pressure propagation,
- axle-end displacement – comparison graph,
- internal energy of tire – comparison graph.

As expected, during the analysis, a pressure wave generated from the HE detonation propagates within the Eulerian vacuum domain. Additionally, soil in which the charge was placed, extends and together with the wave interacts with the suspension system elements. In Fig. 8, selected time points are presented which show the mentioned phenomenon. It should be stressed out that during the charge explosion, buried in the soil, a crater is formed which size depends on HE mass, depth and, most importantly, soil parameters [37].

In Fig. 9 velocity vectors in Eulerian domain are presented for case 1. The highest velocities occur in the nearest areas of tire-pressure wave interaction. Also, the flow around effect is clearly seen and, after a failure of the tire parts, pressure goes inside the wheel and some reflections can be seen. After some time the reflection effect is more evident and stronger which results from the interaction with other suspension system parts.

In Fig. 10, velocity vectors in the Eulerian domain are presented for case 2. The same as previously, the highest velocities occur in the nearest areas of the tire-pressure wave interaction. Also, a flow around effect is clearly seen. One can notice that the characteristic of the pressure wave propagation (vectors directions) is different than previously. In Fig. 10d the flow-around effect is more visible in runflat analysis due to its larger reflection from the structure, whereas in the case 1 major blast energy destroys the tire. It can be expected that after such HE detonation it could be possible to drive a vehicle for some time in order to evacuate from the area of danger.

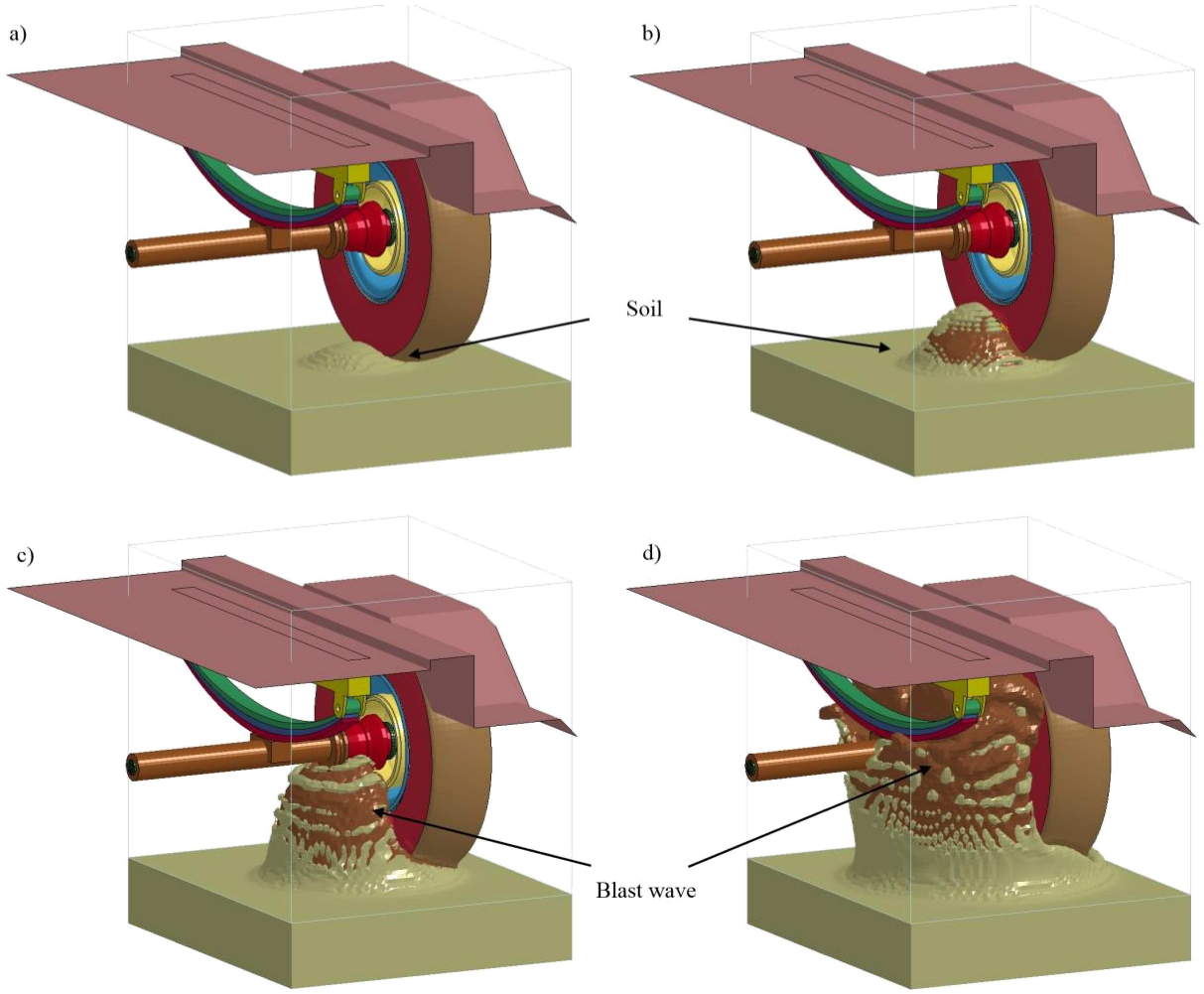

Fig. 8. Soil-blast wave propagation during analysis at selected time points a) $\sim 1.04 \times 10^{-4}$ s, b) $\sim 2.60 \times 10^{-4}$ s, c) $\sim 7.10 \times 10^{-4}$ s, d) $\sim 2.75 \times 10^{-3}$ s

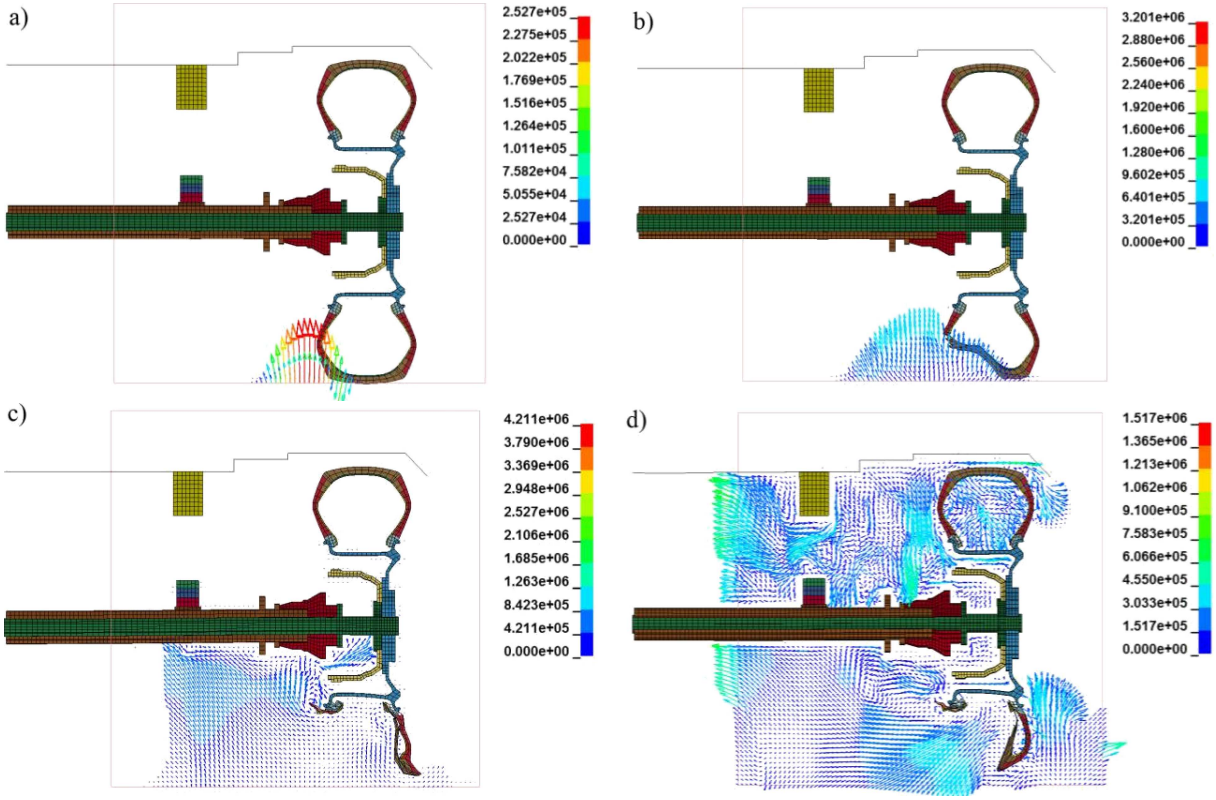

Fig. 9. Velocity distribution [mm/s] within Eulerian domain (case 1): a) $\sim 1.10 \times 10^{-4}$ s, b) $\sim 2.80 \times 10^{-4}$ s, c) $\sim 8.50 \times 10^{-4}$ s, d) $\sim 3.00 \times 10^{-3}$ s

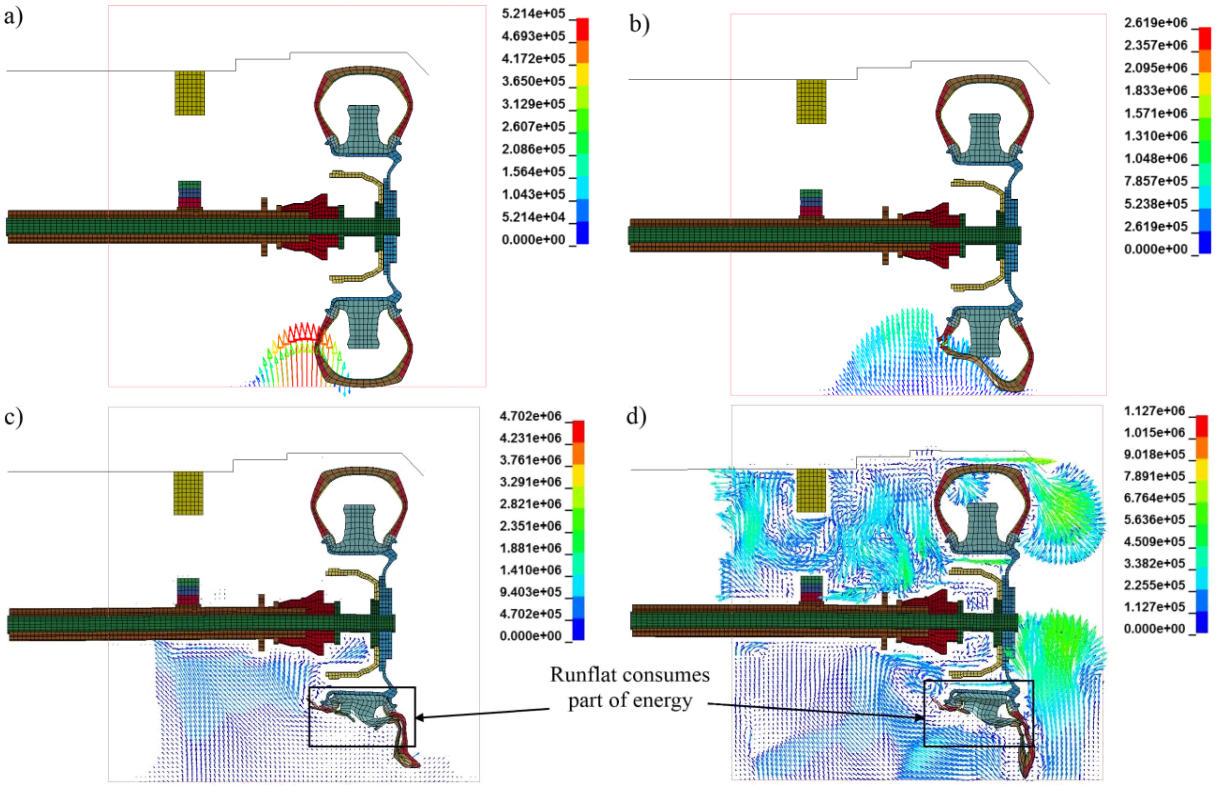

Fig. 10. Velocity distribution [mm/s] within Eulerian domain (case 2): a) $\sim 1.10 \times 10^{-4}$ s, b) $\sim 2.80 \times 10^{-4}$ s, c) $\sim 8.50 \times 10^{-4}$ s, d) $\sim 3.00 \times 10^{-3}$ s

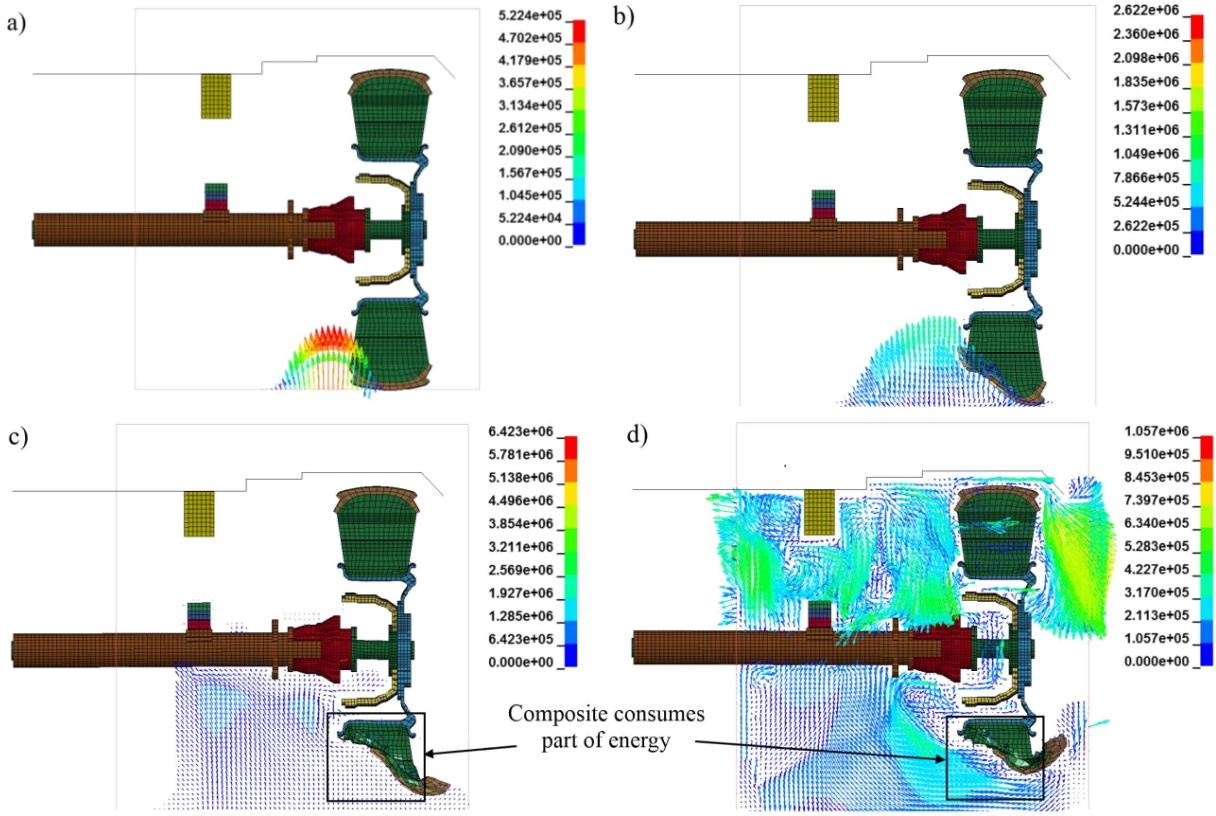

Fig. 11. Velocity distribution [mm/s] within Eulerian domain (case 3): a) $\sim 1.10 \times 10^{-4}$ s, b) $\sim 2.80 \times 10^{-4}$ s, c) $\sim 8.50 \times 10^{-4}$ s, d) $\sim 3.00 \times 10^{-3}$ s

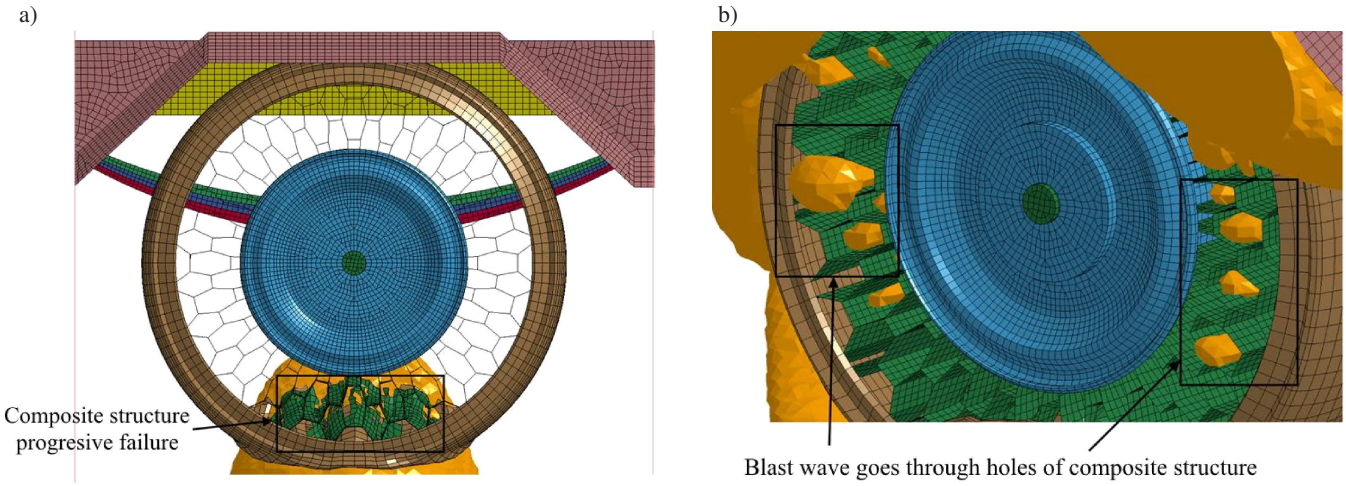

Fig. 12. Composite structure progressive failure (a) and flow-around effect within holes of composite (b)

For the last case Fig. 11 presents velocity vectors in the Eulerian domain. The same effects are observed as before: the highest velocities occur in the nearest areas of the tire-pressure wave interaction and the overall "shape" of velocity vectors is different due to specific geometry and failure characteristic of the honeycomb structure. The intention of such a modification was to dissipate the blast energy as much as possible. Such assumption was found to be correct and the composite structure fulfilled its role. Due to progressive failure the blast energy was constantly dissipated which is clearly presented in below figures. During the next stages of blast wave propagation, part of it goes through holes of the honeycomb structure which also results in blast wave dissipation (Fig. 12).

4.1. Comparative discussion. Based on the presented results, it can be concluded that in every case the suspension system response is different. However, for a detailed study of the results, comparison of HMH stress distribution in the whole model is discussed (at $\sim 3.00 \times 10^{-3}$ s of analyses time). In Figs. 13–15 the fringe levels of HMH stress are

shown. One can see that the pressure wave deals the major damage in similar areas in all cases. The maximum value of HMH stresses was obtained within the rim area. In the analysis with composite insert, the maximum values of *HMH* stress are much lower (419 MPa) than in case 1 (731 MPa) and case 2 (652 MPa). As expected, the most deformed part in all cases is the rim, where the largest plastic strains are observed (∼30%, ∼23% and ∼17%). Greater deformation of the rim in the first two cases demonstrates how much energy was consumed by the composite structure. This is also confirmed in the overall damage of the tire, which is presented in Fig. 16. One can see that, due to crushing and deformation of the honeycomb structure, the tire is relatively less damaged than in the other simulations.

Nevertheless, in all simulated cases no failure was noticed which indicates, as mentioned before, that a large part of the blast energy was consumed by the tire itself. As a consequence, the other parts were not so deformed also due to their geometry, mass as well as stiffer material which were much different comparing to the rubber parts of the tire.

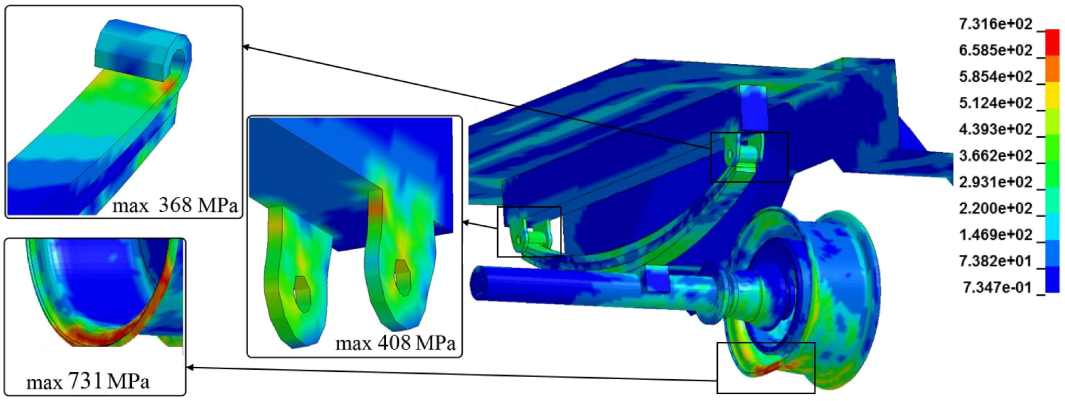

Fig. 13. HMH stress distribution [MPa] with areas of maximum values (case 1)

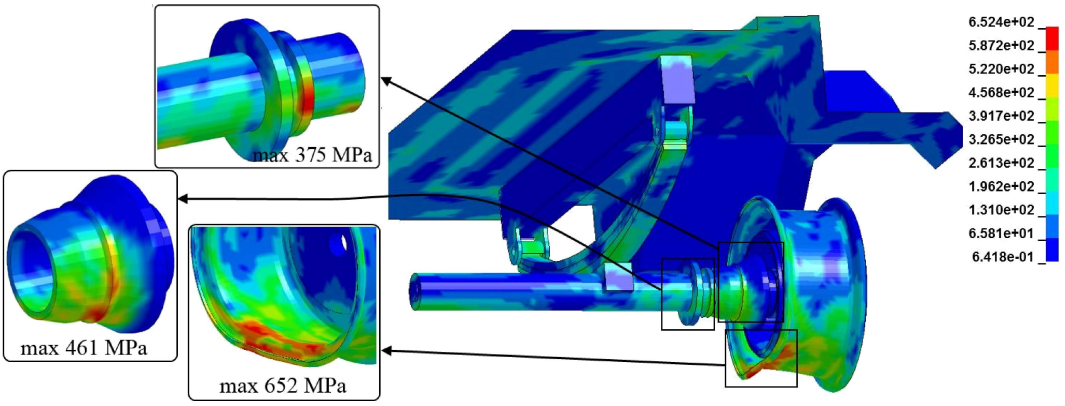

Fig. 14. HMH stress distribution [MPa] with areas of maximum values (case 2)

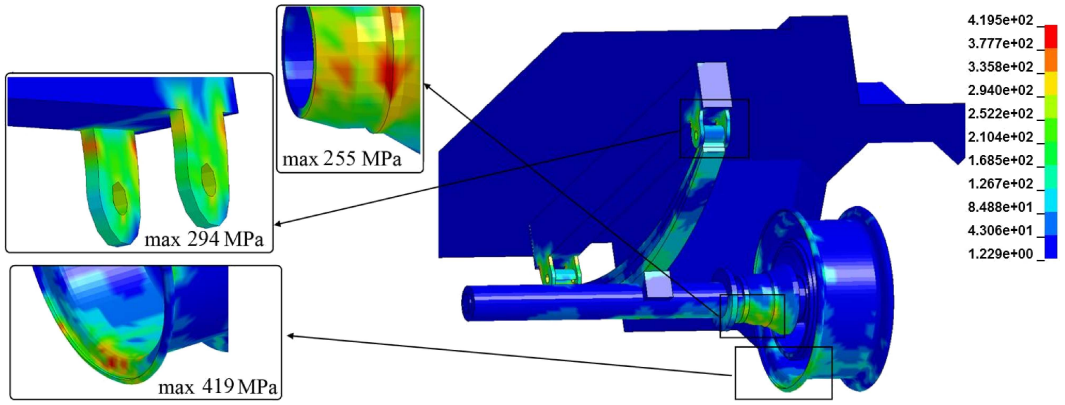

Fig. 15. HMH stress distribution [MPa] with areas of maximum values (case 3)

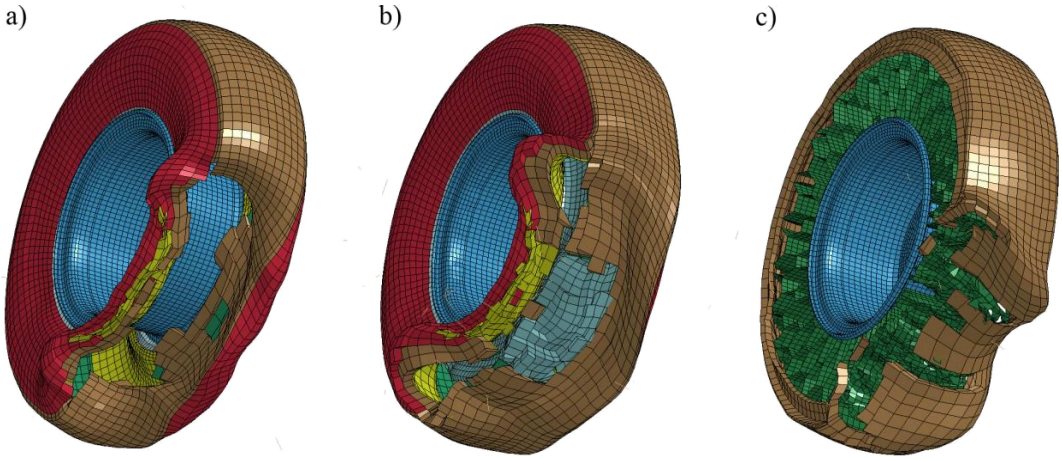

Fig. 16. Damage of tire in all three simulations for same moment of time (at $\sim 3.00 \times 10^{-3}$ s): a) case 1, b) case 2, c) case 3

The above results are also confirmed in the internal energy graph of the tire tread (Fig. 17). For the first two, characteristics are very similar, whereas in third case the energy consumed by the tire is approximately 30% lower than in other simulations. This clearly shows how much energy was dissipated through interaction of the pressure wave with the composite structure.

However, much larger difference can be noticed in the axle-end deflection vs. time graph (Fig. 18). The implementation of both modifications resulted in lowering the deformation of the axle. Despite their influence on the pressure wave was different (runflat: larger overall mass, honeycomb composite: energy dissipation) the axial-end response is similar. Supremacy of the composite manifests in a smaller value of the maximum deflection: 0.56 mm (3.21 mm – case 2, 11.80 mm – case 1), which is also caused by lower mass of the wheel (93.23 kg) compared to case 2 – 101.76 kg (case 1 – 82.83 kg). All described quantities are listed and compared for selected elements of the model for all three simulated cases in Table 8.

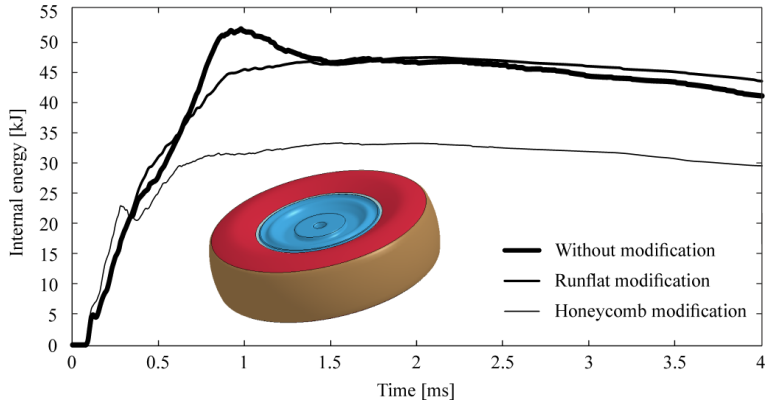

Fig. 17. Tire internal energy comparison for three simulated cases

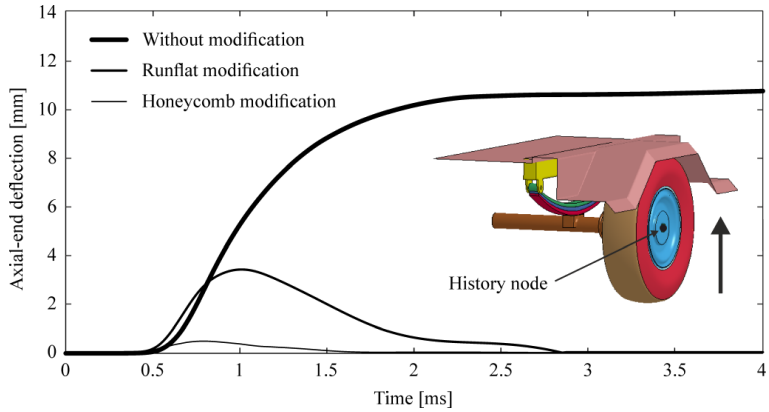

Fig. 18. Axial-end deflection comparison for three simulated cases

Table 8
Comparison table of three simulates cases (max values)

Quantity maximum value	Case 1 (no modification)		Case 2 (runflat insert)		Case 3 (composite structure)	
HMH stress [MPa]	**Rim**	**731.00**	**Rim**	**652.00**	**Rim**	**419.00**
	Spring fixing	408.00	Spring fixing	392.00	Spring fixing	294.00
	Hub	378.00	Hub	461.00	Hub	255.00
Plastic strain [–]	Rim	0.30	Rim	0.23	Rim	0.17
	Spring fixing	0.21	Spring fixing	0.16	Spring fixing	0.07
	Hub	0.14	Hub	0.11	Hub	0.04
Internal energy [kJ]	52.00		47.00		32.50	
Axial-end deflection [mm]	11.0		3.50		0.80	

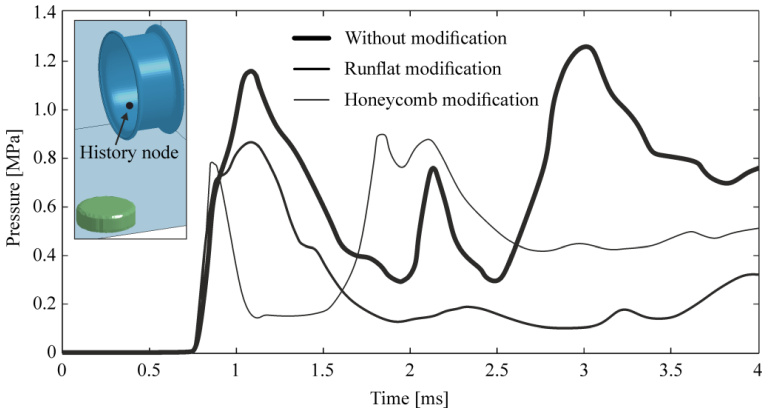

Fig. 19. Pressure history in selected element inside rim

In Fig. 19 pressure history for selected Eulerian element of air domain is presented for all three cases. One can noticed oscillations which are the result of reflections from the rim surface. However, the strengthening effect was only observed in case 1 and case 2, whereas in the simulation with composite insert different tendency can be seen. This is, as mentioned earlier, the result of progressive failure of the composite structure as well as blast energy dissipation.

5. Conclusions

The presented paper covers the problem of numerical modelling of the selected suspension system subjected to the blast wave. In order to minimize the blast energy the modifications of the wheel were proposed which proved to improve strength and resistance of the tire as well as the whole suspension system.

It can be expected that only with the runflat modification it could be possible for a vehicle to drive at some distance, which was also discussed by other authors and confirmed in experimental testing [1]. However, high stress values and relatively large deflection could be a reason of the crew injuries inside the cabin. The most effective solution in terms of blast energy reduction and safety increase is the composite honeycomb structure applied inside the tire, which could provide a possibility to drive but with some difficulties.

In the simulations the most effective and accurate MM-ALE method was adopted which is based on the Lagrangian and Eulerian coupling using the penalty method. This procedure has proved its effectiveness and reliability and that it can handle the interaction between the pressure wave and the complex engineering tire (suspension system) structure. However, a wide range of problems have to be examined and solved: from the most sophisticated constitutive modelling to adopting the proper fluid – structure interaction parameters. Slight modification of only one of them can affect the obtained results. It should be also stated, that no actual tests were carried out. Therefore, presented modelling is only a reference for investigating the problem of blast explosion under a vehicle. The authors intention was to present the possibility of wheel strength improving and testing the selected solutions using numerical methods.

REFERENCES

[1] W. Borkowski and G. Motrycz, "Analysis of IED explosion on carrier road safety", *J. KONES and Powertrain Transport* 19 (4), 75–82 (2012).

[2] G. Motrycz, P. Stryjek, J. Ejsmont, and H. Kalwa, "Tire performance after explosive decompression", *J. Science of the Gen. Tadeusz Kosiuszko Military Academy of Land Forces* 169 (3), 134–144 (2013).

[3] E. Krzystala, A. Mezyk, and S. Kciuk, "Analysis of the impact of explosion on special wheeled vehicles and their crews", *High-speed Tracked Vehicles* 28 (2), 99–110 (2011).

[4] NSA, *Procedures for Evaluating the Protection Levels of Logistic and Light Armoured Vehicles for KE and Artillery Threat*, NSA, Brussels, 2004.

[5] P. Baranowski, J. Malachowski, and T. Niezgoda, "Numerical analysis of vehicle suspension system reponse subjected to blast wave", *Applied Mechanics and Materials* 82, 728–733 (2011).
[6] R.R. Sahu and P.K. Gupta, "Blast diffusion by different shapes of vehicle hull", *Int. J. Automotive Engineering and Technologies* 2 (4), 130–139 (2013).
[7] J.L. Lacome, *Analysis of Mine Detonation, SPH Analysis of Structural Response to Anti-Vehicles Mine Detonation*, LSTC, Livermore, 2007.
[8] G. Toussaint and R. Durocher, "Finite element simulation using SPH particles as loading on typical light armoured vehicles", *Proc. 10th Int. LS-Dyna Users Conf.* 1, 11–18 (2008).
[9] A. Morka, L. Kwasniewski, and J. Wekezer, "Assessment of passenger security in paratransit buses", *J. Public Transportation* 8 (4), 47–63 (2005).
[10] M. Grujicic, B. Pandurangan, I. Haque, B.A. Cheeseman, W.N. Roy, and R.R. Skaggs, "Computational analysis of mine blast on a commercial vehicle structure", *Multidiscipline Modeling in Materials and Structures* 3 (4), 431–460 (2007).
[11] I.R. Cho, K.W. Kim, and H.S. Jeong, "Numerical investigation of tire standing wave using 3-D patterned tire model", *J. Sound and Vibration* 305, 795–807 (2007).
[12] P. Helnwein, C.H. Liu, G. Meschke, and H.A. Mang, "A new 3D finite element model for cord-reinforced rubber composites application to analysis of automobile tyres", *Finite Elements in Analysis and Design* 4, 1–16 (1993).
[13] J.D. Reida, D.A. Boesch, and R.W. Bielenberg, "Detailed tire modeling for crash applications", *Int. J. Crashworthiness* 12 (5), 521–529 (2007).
[14] R.V. Neves, G.B. Micheli, and M. Alves, "An experimental and numerical investigation on tyre impact", *Int. J. Impact Engineering* 10, 685–693 (2010).
[15] P. Baranowski, P. Bogusz, P. Gotowicki, and J. Malachowski, "Assessment of mechanical properties of off road vehicle tire: coupons testing and FE model development", *Acta Mechanica et Automatica* 6 (2), 17–22 (2012).
[16] J. Malachowski, M. Wesolowski, and W. Krason, "Computational study of transport aircraft landing gear during touchdown", *J. KONES and Powertrain Transport* 13 (4), 187–195 (2007).
[17] S.L. Sokolov, "Calculation of the stress- strain state of pneumatic tires by the finite element method", *J. Machinery Manufacture and Reliability* 36 (1), 45–49 (2007).
[18] K.T. Danielson and A.K. Noor, "Three-dimensional finite elements analysis in cylindrical coordinates for nonlinear solid mechanics problems", *Finite Elements in Analysis and Design* 27, 225–249 (1997).
[19] M. Shiraishi, N. Iwasaki, T. Saruwatari, and K. Hayashi, "Developing FE-Tire model library for durability and crash simulations", *Proc.7-th Int. LS-DYNA Users Conf.* 1, 29–36 (2002).
[20] K. Xia, "Finite element modeling of tire/terrain interaction: Application to predicting soil compaction and tire mobility", *J. Terramechanics* 48 (2), 113–123 (2011).
[21] H. Guo, C. Bastien, M. Blundell, and G. Wood, "Development of a detailed aircraft tyre finite element model for safety assessment", *Materials and Design* 53, 902-909 (2014).
[22] S. Kolling, P.A. Du Bois, D.J. Benson, and W.W. Feng, "A tabulated formulation of hyperelasticity with rate effects and damage", *Computational Mechanics* 40, 885–899 (2007).
[23] P. Baranowski and J. Malachowski, "Blast wave and suspension system interaction – numerical approach", *J. KONES Powertrain and Transport* 18 (2), 17–24 (2011).
[24] P. Baranowski and J. Malachowski, "Numerical investigations of terrain vehicle tire subjected to blast wave", *J. KONES Powertrain and Transport* 18 (1), 23–30 (2011).
[25] B. Pondel and J. Malachowski, *Numerical Analysis of Vehicle Tire Operation*, Military University of Technology, Warsaw, 2006, (in Polish).
[26] J. Malachowski, *Modelling and Research of Interaction Between Gas and Pipe Structures Subjected to Pressure Impulse*, Military University of Technology, Warsaw, 2010, (in Polish).
[27] P. Baranowski, "Rubber material study in terms of modelling of terrain vehicle tire subjected to impulse loading", *PhD. Thesis*, Military University of Technology, Warsaw, 2014.
[28] J.O. Hallquist, *LS-Dyna. Theory Manual*, Livermore Software Technology Corporation, Livermore, 2006.
[29] P. Baranowski, J. Janiszewski, and J. Malachowski, "Study on computational methods applied to modelling of pulse shaper in split-Hopkinson bar", *Archives Mechanics* 66 (6), 429–452 (2014).
[30] L. Mazurkiewicz and J. Malachowski, "I-beam structure under dynamic loading – Eulerian mesh density study", *J. KONES Powertrain and Transport* 18 (3), 245–252 (2011).
[31] J. Wang, *Simulation of Landmine Explosion Using LS-DYNA3D Software: Benchmark Work of Simulation of Explosion in Soil and Air*, Aeronautical and Maritime Research Laboratory, Sydney, 2001.
[32] http://www.dynamicrunflats.com/.
[33] http://www.hutchinsoninc.com/CMS/index.php.
[34] A. M .Bothe, "Designed by nature", *Diesel Progress*, 44–45 (2008).
[35] http://www.resilienttech.com/honeycomb-airless-tire-designed-by-nature.
[36] L. Mazurkiewicz, D. Kolodziejczyk, K. Damaziak, J. Malachowski, M. Klasztorny, and P. Baranowski, "Load carrying capacity numerical study of I-beam pillar structure with blast protective panel", *Bull. Pol. Ac.: Tech.* 61 (2), 451–457 (2013).
[37] D. Ambrosini, B. Luccioni, and R. Danesi, "Influence of the soil properties on craters produced by explosions on the soil surface", *Mecanica Computacional* 23, 571–590 (2004).